THE JOURNAL OF PHYSICAL CHEMISTRY B

Article

pubs.acs.org/JPCB

Development of a Thermogravitational Microcolumn with an Interferometric Contactless Detection System

Philipp Naumann,[†] Alain Martin,[‡] Hartmut Kriegs,[†] Miren Larrañaga,[‡] M. Mounir Bou-Ali,*[,‡] and Simone Wiegand*[,†]

[†]Research Center Juelich, ICS-3 Soft Condensed Matter, 52425 Jülich, Germany

[‡]MGEP Mondragon Goi Eskola Politeknikoa, Mechanical and Manufacturing Department, Loramendi 4, Apdo. 23, 20500, Mondragon, Spain

ABSTRACT: We present a new type of thermogravitational (TG) column, a so-called TG microcolumn with transparent windows and a very small sample volume of less than 50 μL. The TG microcolumn has a planar geometry with a thickness of 0.523 ± 0.004 mm, a height of 30 mm, and a width of 3 mm. The concentration difference between two points at different heights is measured with an interferometer using active phase control. From the concentration difference we can determine the thermal diffusion coefficient, D_T, using the refractive index variation with concentration, which has to be determined independently. We studied the three binary mixtures of dodecane, isobutylbenzene, and 1,2,3,4-tetrahydronaphthalene with a concentration of 50 wt % at a temperature of 298 K. The thermal diffusion coefficients agree within a few percent with the proposed benchmark values. In addition we investigated also the binary mixture toluene/*n*-hexane and compare the results with literature values. For the investigated mixtures the typical measurement times were between 30 min and 2 h with an applied temperature difference of ΔT = 6 K.

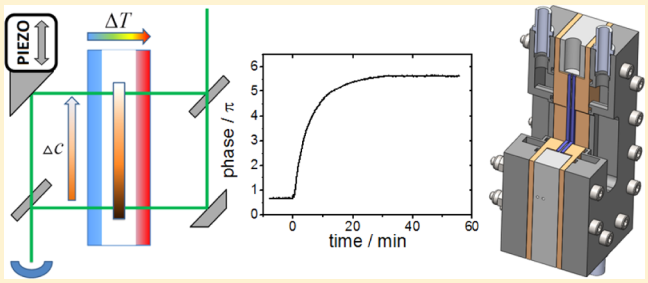

INTRODUCTION

One classical method to study the thermal diffusion or thermodiffusion behavior of binary and multicomponent mixtures is the use of a thermogravitational column (TG).[1] Here, a vertical concentration profile develops due to a combination of thermal diffusion and convection. By combining these two effects, the separation ratio increases compared to a method only relying on the thermal diffusion process.[2] To make a precise measurement possible, the experiment needs to be designed carefully to avoid turbulence. The basic principle was first introduced by Clusius and Dickel[3] and has been evolved into different types of columns. Several designs of TG columns, such as annular TGs[1] and vertical parallelepipedic columns with velocity amplitude determination by laser Doppler velocimetry[4] have been successfully validated in a benchmark with other groups and methods. Nowadays, in conventional TGs a fairly large sample volume of 25 mL and more is required,[5] and small samples of the mixture, typically 1.5 mL, are extracted at different heights from the column after the steady state is reached.[6] These samples are analyzed to determine the composition and thus the separation ratio. For ternary mixtures, two additional properties should be determined (such as density and refractive index) in order to deduce the thermal diffusion coefficients.[7,8] With classical TGs an investigation of expensive substances such as biological systems is often not possible due to the relatively large sample volume which is required to measure the refractive index and density from extracted samples with sufficient accuracy. Therefore, we developed a TG microcolumn with a contactless optical detection system, which works as Mach−Zehnder interferometer. The sample volume is less than 50 μL, so that the investigation of expensive substances or substances which cannot be obtained in large quantities is feasible. Another advantage of the method is the continuous analysis of the concentration profile by measuring the phase difference between two different heights. The possibility to determine the gap width of the microcolumn experimentally once it is mounted is one of the big advantages of our new microcolumn, because the precise knowledge of the width is crucial as the determined thermal diffusion coefficient is proportional to the fourth power of the gap width (eq 5) when calculated from the concentration difference. By use of our optical method, D_T can directly be determined from the phase difference $\Delta\phi$ instead of the measured concentration differences as in conventional TG setups. In the resulting working equation for D_T, the exponent of the gap width reduces to three (eq 6). Therefore, we are less dependent on the precision of fabrication. To validate the new setup, we investigated three binary mixtures of dodecane (DD), isobutylbenzene (IBB), and 1,2,3,4-tetrahydronaphthalene (THN) for a concentration of 50 wt % at a mean temperature of 298 K, which had been used in a benchmark.[9−11] Beside the benchmark systems we investigated also the mixture toluene

Received: June 14, 2012
Revised: November 5, 2012
Published: November 6, 2012

   dx.doi.org/10.1021/jp3098473 | *J. Phys. Chem. B* 2012, 116, 13889−13897

(TOL)/*n*-hexane (HEX) at 298 K and 50 wt %. This organic mixture has been studied by various groups[12−14] with convective and convective-free methods. In the following we discuss the design, construction, and operation of the microcolumn and the interferometer plus its stability. In the appendix we look into some technical details such as the instant when the temperature gradient is applied and the interferometer is disturbed by temperature inhomogeneities within and close to the column.

EXPERIMENTAL SETUP

Materials. We investigated the three binary mixtures consisting of DD (Aldrich, purity 99%), IBB (Aldrich, purity 99%), and THN (Aldrich, purity 99%) at a mean temperature of 298 K. Additionally, we studied also the binary mixture toluene (Aldrich, purity 99%) and *n*-hexane (Aldrich, purity 99%). All chemicals were used without further purification. The investigated mixtures contained 50 wt % of each component. Each sample has been investigated at least five times.

Design and Construction of the TG Microcolumn. The TG microcolumn is composed of two sapphire windows, which are transparent in the visible range of light and have a high thermal conductivity of 34 W/mK at room temperature.[15] The transparency makes it possible to check the cell by eye for defects such as bubbles or dirt. To avoid a distortion of the phase front the material has been cut in the *c* plane (0001). As a thermally insulating gap material we used an advanced polymer material, polyetheretherketone (PEEK), with a very low thermal conductivity of 0.25W/mK,[16] with good chemical resistance and a very low thermal expansion coefficient (50×10^{-6} K^{-1}).[17] Figure 1 shows a sketch of the cell. It consists of

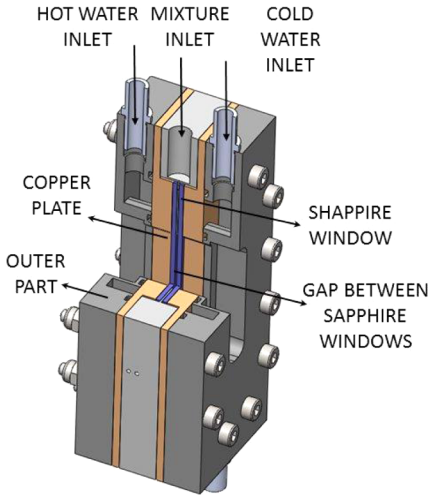

Figure 1. A sketch of the composed microcolumn with a cut in the upper part.

two outer parts made of stainless steel with channels for the thermostated water. For better temperature homogeneity two copper plates in good thermal contact with the two sapphire windows are inserted.

The prepared solutions were slowly inserted from below into the TG microcolumn through two bores in the PEEK part by means of a syringe carefully avoiding bubbles. Once the cell was filled, it was closed by Teflon stoppers to avoid evaporation of the mixture.

On each side a thin channel with a length of 14.5 mm and a width of 250 μm is used to fill the gap. These inlets form dead volumes, which influence the concentration difference between the top and the bottom of the gravitational column and will be discussed in the Numerical Simulation section. The dimensions of the TG microcolumn have been mainly determined by the limits of validity of the Furry−Jones−Onsager (FJO) theory,[18] the limitations on the machining process and experimental conditions such as a sufficient separation ratio and equilibration times in the order of several hours for the systems under investigation.[19] These considerations led to a gap width L_x = 500 μm, a cell height L_{total} = 30 mm, and a width of L_y = 3 mm, so that the aspect ratio is L_{total}/L_x = 60.

Design and Construction of the Interferometer. Figure 2 shows a sketch of the interferometer built around the TG

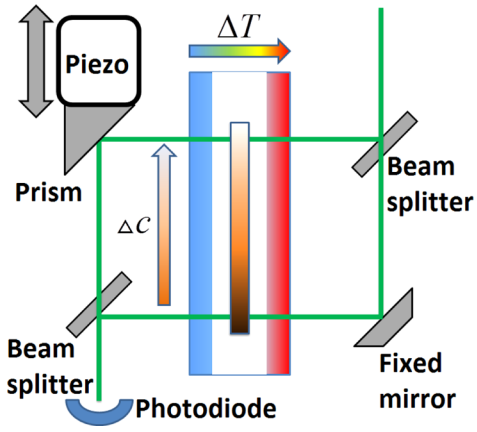

Figure 2. Schematic sketch of the interferometer probing the concentration difference at two different heights of the TG microcolumn with a horizontal temperature gradient. The concentration difference results in a phase shift $\Delta\phi$ of the intensity signal determined by a 2π scan of the prism mounted on the piezo stack.

microcolumn. The microcolumn is mounted inside the interferometer which is built up vertically, splitting the source beam in two parallel beams which probe the TG microcolumn at different heights. The positioning of the cell and the beams is done in a way that one beam passes at the lower end of the window and the other at the upper end. Typically the vertical distance of the two beams is adjusted to 22 mm. To measure at other height differences the vertical position of one of the probing beams can be shifted by moving the two opposing optical elements up- or downward. A He−Ne laser (Melles Griot) with a nominal power of 1 mW and a beam width of 1 mm, operating at 543 nm, is used as a beam source. The typical power at the photodiode (Hamamatsu S2386−8K, active diameter 5.8 mm) is 0.25 mW. Thermostated water from two thermostats (Lauda RE-306) flows through two stainless steel plates mounted at the two sides of the TG microcolumn. To achieve homogeneous starting conditions and to determine the initial phase, the water of both thermostats is mixed and both sides are kept at the same temperature. At time t_0 the temperature gradient is applied by separating the flow from both thermostats.

We use a mirror mounted on a piezo stack (PI P-840-10) to control the phase position while measuring. The piezo is ramped with a step rate of 10 kHz so that we determine the phase from a full 2π scan 2 times per second. This will yield precise knowledge of the initial and final phase positions,

dx.doi.org/10.1021/jp3098473 | J. Phys. Chem. B 2012, 116, 13889−13897

making the determination of the absolute phase shift more exact than measuring only the intensity. The piezo and the recording of the phase shifts (π) are controlled by a computer equipped with an interface card (NI PCI-6014).

The beam width of 1 mm is quite broad compared to the distance between the two probing beams, and the question is whether this will influence the measurements. We can do the following *Gedankenexperiment* by splitting artifically an arbitrary narrow laser beam in one center beam and two *edge beams*, one below and one above the center beam. The vertical concentration profile in the cell is linear, so that the phases of the *edge beams* are shifted by the same amount but in different directions. The resulting *interfering beams* show equal phase shifts stemming from the center and the edges. The relative large area of the photodiode averages over the *beams* recording the same phase as the *center beam* with a slightly lower contrast. Because of the fact that we determine the concentration change by measuring the phase difference, the influence on the measurement should be small as long as the concentration profile is linear over the beam width. In our case the concentration profile is even linear over the entire cell height so there is no influence on the measured phase.

Interferometric Measurement. In an interferometer the intensity varies when the relative phase between the two beams changes. In a simple analysis the phase change can be measured by counting the number of minima and maxima of the varying intensity. To achieve a higher resolution than π the current intensity can be compared to the intensity extrema. This simple method relies on the intensity stability. Therefore, we added an active phase control to our interferometer to achieve a higher precision and reliability. We change the optical path length of one of the beams with a mirror mounted on a piezo and record the modulated intensity (c.f. Figure 3). The resulting intensity

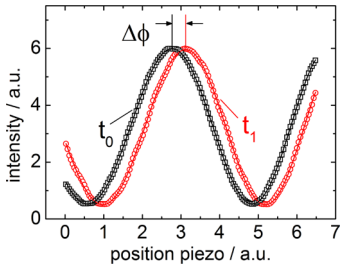

Figure 3. Sketch of the active phase control mechanism. Two intensity scans recorded at two different times t_0 and t_1 (squares and circles) and the fitted sinusoidal curves. The phase shift $\Delta\phi$ is caused by concentration changes.

is fitted to a sinusoidal function which gives a phase value. The curves shown in Figure 3 correspond to the starting time t_0 and a later time t_1. Because of a relative phase shift between the two beams, the signal at t_1 is shifted by $\Delta\phi$ to the right. This full 2π scan takes less than 1 s and is therefore much faster than the expected concentration changes in the microcolumn. We can analyze the phase change by using the forward and the backward movement of the piezo. Both scans give the same phase behavior except for a constant offset caused by the known hysteresis effect of piezos. The interferometer with active phase control is less sensitive to intensity fluctuations caused by mechanical disturbances, and we do not need the reference information about the actual intensity extrema to be measured in advance.

Characterization of the Cell. The gap width of the microcolumn has been determined with a microscope setup, focusing a probing beam onto the surface and detecting the reflected signal. The objective used (10× Mitutoyo) has a long working distance of 33.8 mm and a very small focus depth of 3.58 μm. A principle sketch of the setup is shown in Figure 4a. When the beam is focused on an interface, the reflected beam forms a sharp focused spot and the intensity is on its local maximum. We record the focus shift from the first window-cell interface to the second via an elevator stage. The precision of the height reading is better than 0.5 μm. With this method we determined the average cell thickness to be 523 μm with an uncertainty of 4 μm. The roughness of the inner walls is smaller than the uncertainty.

THEORETICAL APPROACHES

Determination of the Phase Shift due to Concentration. As sketched in Figure 2 we are probing the relative phase difference along the TG microcolumn at two different heights. The phase ϕ between the two beams corresponds to their optical path lengths s_{top} and s_{bottom} inside the column gap via

$$\phi = k(s_{top} - s_{bottom}) \tag{1}$$

with the wave vector $k = (2\pi)/\lambda$ and λ, the wavelength of the laser, assuming a perfectly frequency stable laser. A change in the optical path lengths, Δs_{top} and Δs_{bottom} at the top and bottom, respectively, leads to a change in the phase $\Delta\phi$

$$\Delta\phi = k(\Delta s_{top} - \Delta s_{bottom}) \tag{2}$$

We assume here that the change in refractive index along the column in vertical direction depends only on the concentration difference between top and bottom beam positions. Supported by the simulations we suppose that the temperature changes linearly over the gap). Therefore, the mean temperature is in the middle of the gap, and it is a constant as function of the height. Looking at the horizontal variation of the refractive index we have on the warm side a slightly lower refractive index compared to the middle and at the cold side a slightly higher refractive index compared to the middle. Because of the linearity of the temperature the averaged refractive index probed by the laser beam corresponds to the value in the middle, which is constant over the height of the cell. Therefore we consider that all observed changes in the refractive index are due to concentration changes. Since the change of the optical path results from the change in refractive indices, Δn_{top} and Δn_{bottom} at the top and bottom, respectively, one can write

$$\Delta\phi = kL_x(\Delta n_{top} - \Delta n_{bottom}) = kL_x\Delta n \tag{3}$$

$$\Leftrightarrow \Delta n = \Delta\phi(kL_x)^{-1}$$

with the gap width L_x and the refractive index difference Δn between top and bottom. Additionally, we neglect the phase changes between the top and bottom beam caused by refractive index change and thermal expansion of the sapphire windows (c.f. Figure 1) and the air around the cell due to the temperature gradient, since both beams are affected in the same way. Dividing both sides of (eq 2) by Δc and replacing $\Delta n/\Delta c$ with $(\partial n/\partial c)_{p,T}$, we obtain an expression for Δc

$$\Delta c = \frac{1}{kL_x}\left(\frac{\partial n}{\partial c}\right)^{-1}_{p,T}\Delta\phi \tag{4}$$

dx.doi.org/10.1021/jp3098473 | J. Phys. Chem. B 2012, 116, 13889−13897

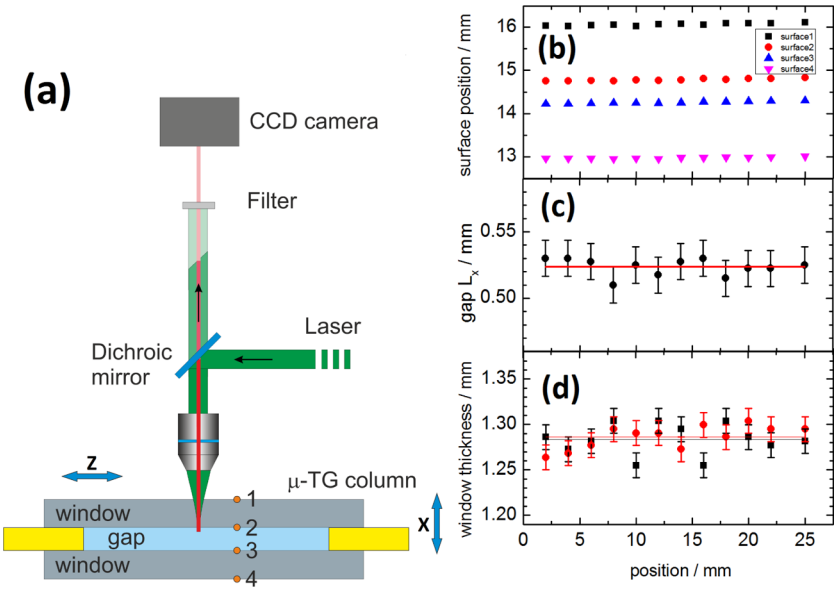

Figure 4. Optical tweezers setup to determine the position of the sapphire surfaces. The cell can be moved in the *x*- and *z*-directions on a micrometer stage. (b) Position of the different surfaces along the cell. (c) The calculated gap width and the width of the (d) sapphire windows as function of the cell height.

The refractive index increment $(\partial n/\partial c)_{p,T}$ can be determined independently. Furthermore, we would like to point out that due to continuous observation of $\Delta\phi$ also phase differences larger than 2π can be detected.

Determination of the Concentration Change. We use the FJO theory[18,20] to calculate the concentration difference at the steady state at two points separated by L_z to

$$\Delta c = 504\frac{\nu}{\alpha g}D_T c_0(1 - c_0)\frac{L_z}{L_x^4} \tag{5}$$

where c_0 is the initial mass fraction concentration of the reference component, ν is the kinematic viscosity, α is the thermal expansion coefficient, L_z is the vertical distance between the probing laser beams (22 mm), D_T the thermal diffusion coefficient, and g the gravity acceleration. In the derivation it is used that the initial concentration c_0 changes only slightly, so that D_T and also D can still be treated as a constant. This assumption might break down, if large concentration changes occur. Combining eqs 4 and 5 gives the thermal diffusion coefficient

$$D_T = \frac{1}{504}\frac{\alpha g}{k\nu}\frac{1}{c_0(1 - c_0)}\frac{L_x^3}{L_z}\left(\frac{\partial n}{\partial c}\right)_{p,T}^{-1}\Delta\phi \tag{6}$$

Because of the fact that we do have a method which measures the phase continuously, we might also look at the temporal behavior of the transient concentration difference. This is given by[21]

$$\Delta c = \Delta c_\infty(1 - ae^{-t/t_r}) \tag{7}$$

It needs to be pointed out that eq 7 is only satisfied for times t larger than one-third of the relaxation time t_r because it corresponds only to the first term of an infinite series. Another shortcoming of eq 7 is that an ideal infinitely sharp switching of the temperature gradient is assumed, which practically cannot be achieved. In the future we will develop an experimental procedure to obtain the molecular diffusion coefficient from the transient signal.

NUMERICAL SIMULATIONS

Numerical Validation of the TG Microcolumn. To validate the proposed geometry for the TG microcolumn, a numerical study using ANSYS-Fluent software[22] is made. The simulations are performed using a finite volume (illustrated in Figure 5) method in 3D (FVM) based on fluid flow solutions under the assumption of an incompressible fluid and laminar flow under atmospheric pressure.

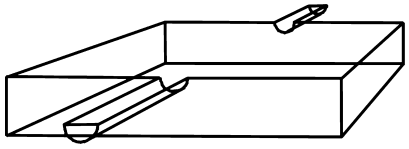

Figure 5. A sketch of the cell volume including the considered dead volumes, which are used for filling the microcolumn.

The model covers the Fickian mass, the thermal diffusion, and the Navier–Stokes equation, whereas the density changes in the fluid with concentration and temperature are covered by the Boussinesq approximation[23]

$$\rho = \rho_0(1 - \alpha(T - T_0) + \beta(c - c_0)) \tag{8}$$

where ρ is the local density of the mixture, ρ_0 is the density of the homogeneous mixture, T_0 is the mean temperature, $\alpha = -(1/\rho)(\partial\rho/\partial T)_{p,c}$ is the thermal expansion coefficient and $\beta = +(1/\rho)(\partial\rho/\partial c)_{p,T}$ is the mass expansion coefficient. The value of the mass and thermal expansion coefficient are experimentally determined.[24] We used no-slip boundary conditions and applied a constant temperature gradient of 5 K perpendicular to the gravity field.

The governing equations are solved using a pressure-based implicit simple velocity-pressure coupling scheme with a double-precision module. The second-order numerical discretization scheme is used for pressure, density, momentum, and mass flux to avoid numerical instabilities. The iterative convergence criteria is set to 10^{-9} for all solution variables.

dx.doi.org/10.1021/jp3098473 | J. Phys. Chem. B 2012, 116, 13889–13897

For the preprocessing of the geometry Gambit[25] is used, where the geometry of the gap (523 μm × 3 mm ×30 mm) was defined. This 3D computational domain consists of nonuniformly spaced hexahedral mesh cells. A very fine mesh resolution was used with 720 000 hexahedral cells to have a realistic representation of the concentration gradients.

Simulation Results. For the numerical validation of the microcolumn, the TG effect in the steady state is analyzed using a reference mixture TOL/HEX at a mass fraction of 0.5167 and at T = 298 K. Table 1 lists the parameters for the TOL/HEX mixture. Köhler and Müller measured only at T = 296 K and higher temperatures so that D_T and D at T = 298 K have been obtained by linear interpolation.[12]

Table 1. Experimental Density, ρ_0, Dynamic Viscosity, μ, Mass Expansion Coefficient, β, and the Thermal Diffusion Coefficient, D_T, for the Mixture TOL/HEX with a Mass Fraction of 0.5167 at T = 298 K Used in the Numerical Simulation

ρ_0/kg/m^3	μ/Pa·s	α/K^{-1}	β	$D_T/10^{-12}$ m^2/sK	$D/10^{-9}$m^2/s
748.19	3.861	1.23	0.275	13.7 [ref 13]	2.78 [ref 13]
				13.2 [ref 14]	2.85 [ref 12]
				14.0 [ref 12]	

For the TOL/HEX mixture with c_0 = 0.5167 the steady state temperature, velocity, and concentration profiles obtained from numeric simulations are shown in Figure 6 and Figure 7. Figure 7a shows the temperature profile within the gap which decays linearly from the warm to the cold side. Figures 6 and 7b show the velocity and the toluene concentration profiles inside the gap at the midheight of the microcolumn at 15 mm. The velocity (c.f. Figure 7b) has a cubical profile while the concentration profile (c.f. Figure 6) has to be described by a polynomial of the fifth order. Figure 7c show the distribution of the concentration referring to the densest component (TOL) in the stationary state. Along the microcolumn the results show an increase in the concentration of the densest component (TOL) in the lower and of the lightest component (HEX) in the upper parts of the column. The profiles obtained in the microcolumn are those predicted by the TG theory.[26,27]

Table 2 summarizes the results of numerical simulation and compares the concentration difference and the thermal diffusion coefficient in the steady state with the experimental values. The simulation results agree within a few percent with the experimental values and the mean experimental value agrees within 1%. The excellent agreement between the simulation results and the experimental values shows that the design fulfills the conditions of the FJO theory.

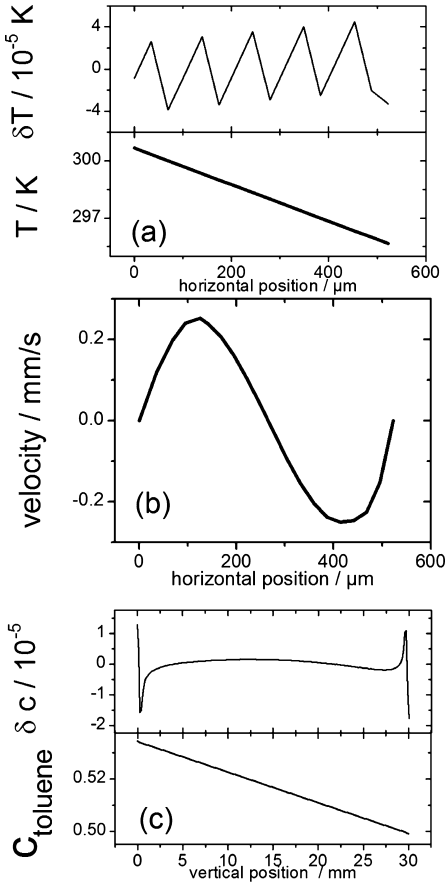

Figure 7. Numerical simulation results for the binary mixture TOL/HEX at the stationary state. (a) Temperature profile within the microcolumn gap. The upper part shows the deviations from a linear fit. (b) Velocity profile within de microcolumn gap at a height of 15 mm. (c) The vertical concentration distribution profile of the TOL mass fraction in the middle of the gap along the microcolumn. The upper part shows again the deviations from a linear fit.

Additionally, we analyzed numerically the effect on the concentration difference probably caused by dead volumes at the inlet and outlet. The considered dead volumes are in the order of 3.625 μL stemming from two channels with a diameter of 250 μm and 14.5 mm in length. Figure 5 shows the model used. As shown in Table 3, the obtained concentration difference from the simulation Δc_{fluent} agrees within 1% with

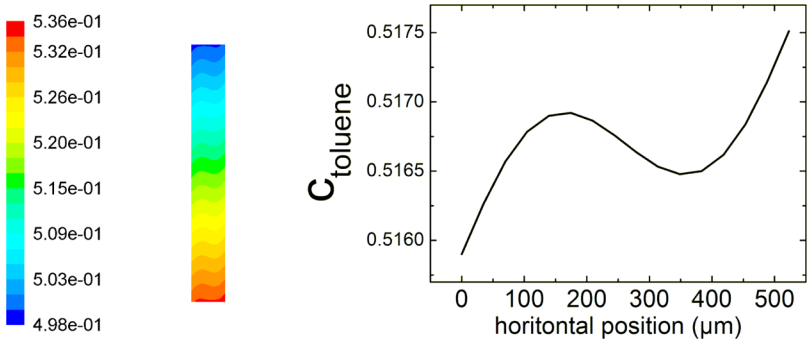

Figure 6. Numerical simulation results of the toluene mass fraction profile in the binary mixture TOL/HEX. The left figure shows the profile over the entire height of the microcolumn. The right figure is a plot of the concentration profile at a height of 15 mm at the stationary state.

dx.doi.org/10.1021/jp3098473 | J. Phys. Chem. B 2012, 116, 13889−13897

Table 2. Comparison between Experimental and Numerical Simulation Results of the Stationary Separation under the TG Effect for the New Design of the Microcolumn for the Mixture TOL/HEX with a Mass Fraction of 0.5167[a]

L_z/ mm	Δc (eq 5)	Δc_{fluent}	dev/ %	$D_{T_{exp}}$/ 10^{-12} m^2/sK	$D_{T_{fluent}}$/ 10^{-12} m^2/sK	dev/ %
30	0.0295	0.0297	<1	13.63	13.74	<1
22	0.0216	0.0218	<1	13.63	13.76	<1

[a] D_T is the average of the individual literature values listed in Table 1.

the calculated concentration difference Δc (eq5). The determined thermal diffusion coefficients for TOL/HEX, THN/IBB, IBB/DD, and THN/DD mixtures at a mass fraction of 50% at T = 298 K agree also within a few percent with the simulation results obtained for a gap of 523 μm including the dead volume effect.

RESULTS AND DISCUSSION

Figure 8 shows a typical time development of the phase for the system TOL/HEX and THN/DD at an average temperature of T = 298 K and a temperature difference of ΔT = 6 K over the gap of the cell. At time t = 0 the temperature gradient is applied while at earlier times both sides of the cell are kept at an average mixing temperature, T_{mix}, which leads to a constant phase after some settling time of the order of an hour. Once the temperature gradient is applied, the phase shows an exponential increase until it reaches a plateau value. The phase difference is determined by the difference of the plateau value in the steady state and the phase at the baseline before switching on the temperature gradient. In all our experiments this phase change in the jump was of the order of 0.2 π, and its origin will be discussed in the Appendix. The so-determined phase difference is used in eq 6 to calculate the thermal diffusion coefficient, D_T. The obtained values for the four systems are listed in Table 4 and shown in Figure 9 in comparison with literature values. For most of the systems the deviations are below or around 6%. The absolute uncertainty was below 0.6 × 10^{-12} m^2 s^{-1} K^{-1}. With this new TG microcolumn design in combination with the interferometric detection with one wavelength we surrender a strong point of the TGs, namely, the investigation of ternary mixtures. In addition we employ very small sample volume of less than 50 μL, with similar measurement times compared to the conventional TGs of 30 min up to 2 h for the investigated mixtures. Both the design and the measurement system developed in this work for the new TG microcolumn installation is well suited for biological systems. The transparent windows of the TG microcolumn have several advantages. First, a precise determination of the gap width over the entire height of the TG microcolumn is possible. This is especially important, because the thermal diffusion coefficient, D_T depends on the gap width to the power of three (c.f., eq 6) for our optical system. So far we have only studied organic mixtures, but the setup should also work for aqueous solutions. Because of the higher surface tension of water, special care needs to be taken in order to avoid air bubbles in the cell. Another nice feature of the TG microcolumn is that we can monitor the concentration change as function of time. In principle it should therefore also be possible to determine the diffusion constant D in the same setup. In the present design, however, we were not able to obtain sufficiently accurate values for D. The largest problem is the uncertainty in ΔT, which needs to be obtained at the inside of the sapphire windows. We hope that we can analyze in the near future the time dependence of the concentration to obtain also the Soret

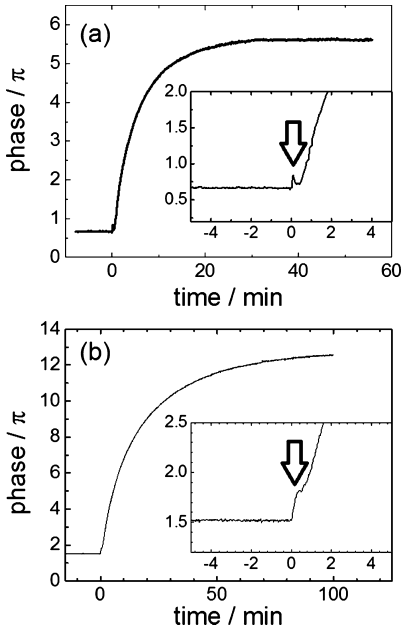

Figure 8. (a) Typical experimental results for phase shift between top and bottom for the mixture TOL/HEX and (b) THN/DD with a mass weight fraction of 50% as function of time. The time base has been chosen in such a way that at time zero the temperature gradient has been enabled. The inset shows the phase close to the turn-on time. The origin of the fast jump in the signal will be discussed in detail in the Appendix.

Table 4. Thermal Diffusion Coefficients Determined for Four Binary Mixtures with 50 wt %[a]

mixture	D_T/(this work) 10^{-12} m^2/sK	D_T/(literature) 10^{-12} m^2/sK	dev/ %
TOL-HEX	13.0 ± 0.35	13.6 [avg]	−0.44
THN-DD	5.87 ± 0.23	5.9 [ref 9]	−0.50
THN-IBB	2.63 ± 0.01	2.8 [ref 9]	−6.07
IBB-DD	3.91 ± 0.15	3.7 [ref 9]	+5.68

[a] All measurements have been performed at 298 K. The error is the variance of the mean from five individual measurements.

Table 3. Experimental and Numerical Results for the Investigated Binary Mixtures at T = 298 K and a Mass Fraction of c = 0.5[a]

mixture	Δc (eq 5), L_z = 22 mm	Δc_{fluent}, L_z = 22 mm	dev/%	$D_{T_{exp}}/10^{-12}$ m^2/sK	$D_{T_{sim}}/10^{-12}$ m^2/sK	dev/%
TOL-HEX	0.0213	0.0214	0.47	13.6 [avg, ref 12−14]	13.56	−0.29
THN-DD	0.0451	0.0453	0.44	5.90 [ref 9]	5.93	0.50
THN-IBB	0.0180	0.0177	−1.66	2.80 [ref 9]	2.78	−0.71
IBB-DD	0.0207	0.0206	−0.48	3.70 [ref 9]	3.68	−0.54

[a] In all simulations the dead volume caused by the inlet and the outlet has been considered.

dx.doi.org/10.1021/jp3098473 | J. Phys. Chem. B 2012, 116, 13889−13897

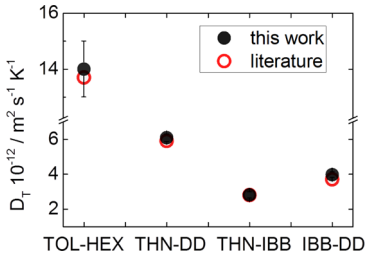

Figure 9. The thermal diffusion coefficient, D_T, for the four studied systems in comparison with literature values. The largest absolute deviations are found for the system TOL/HEX, while the largest relative deviation of around 6% is found for the system THN-IBB.

coefficient, S_T, but this might also require a more sophisticated model for the data analysis.

Compared to other optical detection methods such as thermal diffusion forced Rayleigh scattering (TDFRS)[28,29] or beam deflection (BD)[10,30] the sample volume of 50 μL is very small. The equilibration times are comparable with BD but much slower than in the TDFRS experiments. One drawback of the method is that we are not capable to determine also the diffusion coefficient D using eq 7, because the experimental data show systematic deviations from a simple exponential function. The operating expenses are much lower than in the case of the TDFRS and comparable with the BD. This method might open up other possibilities by combining it with a microscope and fluorescent detection methods. This new method will also be useful for further benchmark campaigns as a convective method in combination with optical detection.

In conclusion we can state that the TG microcolumn is a nice compact device which allows reliable, contactless measurements of the thermal diffusion coefficient, D_T. The typical deviations from the literature values found are in the order of 5% (c.f., Table 4), which is comparable with the deviation found in the benchmark.[9]

APPENDIX

As mentioned in the Results and Discussion section we observe always a fast phase jump shortly after switching on the temperature gradient. In the following section we will discuss this issue and will relate it to a slight asymmetry in the formation of the temperature gradient.

Characterization of the Temperature Switching

Before the measurement starts, we mix the water of the two thermostats, which are kept at different temperatures T_{cold} and T_{warm}. We adjust the flows of the two thermostats so that the temperature of the mixed water corresponds to the average of the two temperatures $T_{mean} = 0.5(T_{cold} + T_{warm})$. Practically, small deviations of the order of $\Delta T = 0.1$ K are detected. This leads to a small temperature difference to the mean temperature, T_{mean}, of the cell prior the temperature gradient and causes a small horizontal asymmetry in the $(\partial n/\partial T)_{p,T}$ contributions. If the thickness of the gap and the windows between top and bottom are equal, this affects top and bottom in the same way, so that changes in the phases should cancel.

Figure 10 shows the temperatures on the cold and warm sides as a function of time after the temperature gradient has been switched on. The temperatures have been measured with an infrared camera (FLIR T400) at the surface of the sapphire windows, which has been covered with a 100-μm Teflon foil to avoid reflections. Because of the insulation of the Teflon foil the temperature reading will be a bit lower compared to the

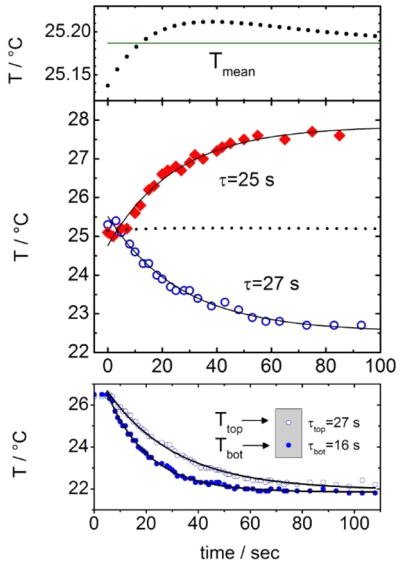

Figure 10. Top: temperature at the outside of the sapphire windows at the two sides (warm side, filled diamonds; cold side, open circles) of the TG microcolumn filled with toluene as function of time measured by means of an infrared camera. The upper graph shows that due to different time constants for the warm and the cold side there is a small overshot in the mean temperature (small dots) as function of time. Bottom: development of the temperature at the bottom and at the top of the cell measured at the covered metal surface. The temperature equilibrates at the bottom of the cell much faster than at the top, so that for a short time a vertical temperature gradient in the order of 0.2−0.3 K is established. The solid lines are exponential fits with time constants given in the graph.

temperature at the outside of the sapphire window, but this will affect both sides in the same way. Also the surrounding metal parts have been taped to prevent reflections at the metal surfaces, which could influence the temperature reading. Figure 10 shows the time development of the temperatures on the warm and cold side, which can be described by an exponential increase and decrease, respectively. Typical time constants of an exponential fit to reach the final values T_{cold} and T_{warm} are 27 and 25 s, respectively, indicating that heating is slightly faster than cooling. This leads as in the upper graph of Figure 10 shown to a slight overshot of the average temperature, T_{mean}. But this effect will also influence the top and the bottom in the same way so that those contributions cancel.

By thermal analysis with the infrared camera, we have seen that during the initial state of applying the temperature gradient the temperature propagates from the bottom to the top, which means that the final temperature at the bottom is reached earlier compared to the top. The lower graph of Figure 10 shows the temperature at the top and bottom measured at the metal surface of the cell. Because of the small window of a width of 3 mm we were not able to obtain reliable measurements at two different height positions directly at the sapphire windows. As seen in the figure the time constants between top and bottom differ substantially. Typical exponential time constants at the bottom and at the top of the cell are 16 and 27 s, respectively. This is indeed a problem of the present setup and leads to phase shift between the bottom and the top present in the beginning of the experimental phase curves. This difficulty can be solved by using a cross-flow in the microcolumn similar to the circulating

dx.doi.org/10.1021/jp3098473 | J. Phys. Chem. B 2012, 116, 13889−13897

water loops used by Zhang et al.[13] or by imaging the phase profile over the entire height.

Stability and Response of the Interferometer

The precision of the setup depends strongly on the stability of the interferometer. The drift should be very small over the measurement time. A typical measurement time is of the order of 30 minutes to 2 h depending on the system. A small drift has little influence and can be subtracted from the measured signal. To achieve a very small drift, we have to insulate the laser beam paths from temperature changes by insulating the cell and the tubes. This will reduce the effect but not cancel it out completely. The interferometer mirrors are mounted on vertical pillars. Care needs to be taken to have stable temperature conditions taking into account heat sources and fluctuations.

A typical example for the time dependence of pure THN is shown in Figure 11b. At short times when no temperature gradient is applied, we observe a constant drift of the phase. After 10 minutes a temperature gradient is applied, and the phase changes rapidly within a minute and approaches then a constant drift rate. When the temperature gradient is switched off, we observe the reverse behavior. A similar jump occurs also in the empty cell and during the regular measurements and is always in the order of 0.2π. Therefore, we assume that it is related to an asymmetry in the setup, but the reason is not fully understood. In the last section we discussed a small vertical temperature gradient and the temporal change of the mean temperature in Figure 11b and the top portion of Figure 10, respectively. The maximal temperature difference between top an bottom is of the order of 0.2−0.3 K; with a typical $(\partial n/\partial T)_{p,c} = 5 \times 10^{-4}$ K^{-1}, we obtain a phase shift of the order of 0.2π−0.3π, which corresponds to the typical observed values of 0.2π. On the other hand it is also possible that the two beams are slightly deflected leading to a shift of the interference pattern, which results then into an intensity change. We want to clarify this issue in the future by comparing different microcolumns.

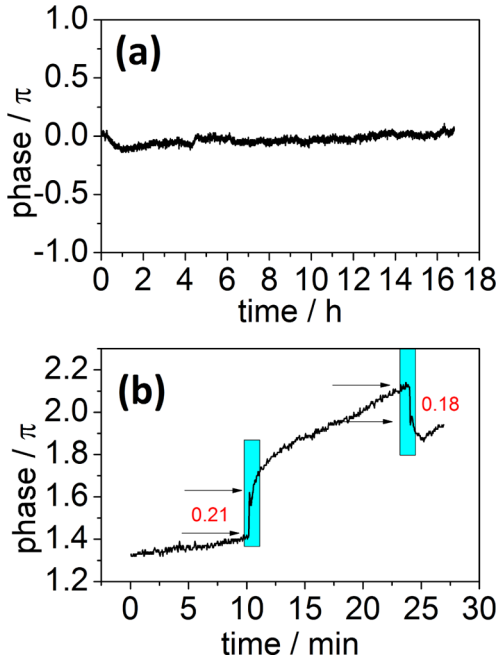

Figure 11. (a) Phase drift as function of time. After equilibration within the first hour, the phase drifts with a rate 0.0064 π/h. This corresponds to a drift of less than 0.02 π for a measurement time of 3 h, which results for IBB/THN, the system with the weakest measurement signal, in a relative error of 1%. (b) Phase response in pure THN, when the temperature gradient is switched on and off, respectively.

AUTHOR INFORMATION

Corresponding Author

*E-mail: mbouali@mondragon.edu (M.M.B.-A.); s.wiegand@fz-juelich.de (S.W.).

Notes

The authors declare no competing financial interest.

ACKNOWLEDGMENTS

We thank Jan Dhont for his constant interest and many helpful discussions. Special thanks to Axel Ackens, who lended the infrared camera to us. We thank also Christoph July and Peter Lang for the use of their tweezers setup for the determination of the cell thickness and we show our gratitude to Michael Klein for a first outline of the interferometer. The Jülich group acknowledges financial support due to the DAAD PPP program and the Deutsche Forschungsgemeinschaft Grant Wi 1684. The MGEP group thanks the TEDIBIO integrated action project (No. DE 2009-0024) and LOCUS2 (No. BIO2011-30535-C04-04) project from the Spanish Goverment, as well as the GOVSORET3 (No. PI2011-22), MIDIAG project, and the project of Fluids Mechanics Groups (IT557-10) of the Basque Country Government.

REFERENCES

(1) Bou-Ali, M. M.; Valencia, J. J.; Madariaga, J. A.; Santamaria, C.; Ecenarro, O.; Dutrieux, J. F. *Philos. Mag.* **2003**, *83*, 2011−2015.

(2) Platten, J. K.; Bou-Ali, M. M.; Dutrieux, J. F. *J. Phys. Chem. B* **2003**, *107*, 11763−11767.

(3) Clusius, K.; Dickel, G. *Naturwissenschaften* **1938**, *26*, 546−546.

(4) Platten, J. K.; Bou-Ali, M. M.; Dutrieux, J. F. *Philos. Mag.* **2003**, *83*, 2001−2010.

(5) Blanco, P.; Bou-Ali, M. M.; Platten, J. K.; de Mezquia, D. A.; Madariaga, J. A.; Santamaria, C. *J. Chem. Phys.* **2010**, *132*, 114506 1−6.

(6) Dutrieux, J. F.; Platten, J. K.; Chavepeyer, G.; Bou-Ali, M. M. *J. Phys. Chem. B* **2002**, *106*, 6104−6114.

(7) Bou-Ali, M.; Platten, J. K. *J. Non-Equil. Thermody.* **2005**, *30*, 385−399.

(8) Leahy-Dios, A.; Bou-Ali, M. M.; Platten, J. K.; Firoozabadi, A. *J. Chem. Phys.* **2005**, *122*, 234502 1−12.

(9) Platten, J. K.; Bou-Ali, M. M.; Costeseque, P.; Dutrieux, J. F.; Köhler, W.; Leppla, C.; Wiegand, S.; Wittko, G. *Philos. Mag.* **2003**, *83*, 1965−1971.

(10) Königer, A.; Meier, B.; Köhler, W. *Philos. Mag.* **2009**, *89*, 907−923.

(11) Mialduna, A.; Shevtsova, V. *J. Chem. Phys.* **2011**, *134*, 044524 1−12.

(12) Köhler, W.; Müller, B. *J. Chem. Phys.* **1995**, *103*, 4367−4370.

(13) Zhang, K. J.; Briggs, M. E.; Gammon, R. W.; Sengers, J. V. *J. Chem. Phys.* **1996**, *104*, 6881−6892.

(14) Bou-Ali, M. M.; Ecenarro, O.; Madariaga, J. A.; Santamaria, C. M.; Valencia, J. J. *J. Phys.: Condens. Matter* **1998**, *10*, 3321−3331.

(15) Burghartz, S.; Schulz, B. *J. Nucl. Mater.* **1994**, *212*, 1065−1068.

(16) Choy, C. L.; Kwok, K. W.; Leung, W. P.; Lau, F. P. *J. Polym. Sci., Part B: Polym. Phys.* **1994**, *32*, 1389−1397.

(17) Choy, C. L.; Leung, W. P. *J. Polym. Sci., Part B: Polym. Phys.* **1990**, *28*, 1965−1977.

(18) Furry, W. H.; Jones, R. C.; Onsager, L. *Phys. Rev.* **1939**, *55*, 1083−1095.

(19) Martin, A.; Bou-Ali, M. M.; Gandarias, E.; Aristimuño, P.; Wiegand, S. EP12382015, Europe, 2012.

(20) Majumdar, S. D. *Phys. Rev.* **1951**, *81*, 844−848.
(21) Valencia, J. J.; Bou-Ali, M. M.; Platten, J. K.; Ecenarro, O.; Madariaga, J. M.; Santamaria, C. M. *J. Non-Equil. Thermody.* **2007**, *32*, 299−307.
(22) *Ansys Inc*; Ansys-Fluent 13.0, Lebanon, USA, 2010.
(23) Platten, J. K.; Chavepeyer, G. *Int. J. Heat Mass Transf.* **1976**, *19*, 27−32.
(24) Blanco, P.; Bou-Ali, M. M.; Platten, J. K.; Urteaga, P.; Madariaga, J. A.; Santamaria, C. *J. Chem. Phys.* **2008**, *129* (174504), 1−6.
(25) *Ansys Inc*; Gambit 2.4.6, Lebanon, USA, 2010.
(26) Valencia, J.; Bou-Ali, M. M.; Ecenarro, O.; Madariaga, J. A.; Santamaria, C. M. *Thermal Nonequilibrium Phenomena in Fluid Mixtures* **2002**, *584*, 233−249.
(27) Madariaga, J. A.; Santamaria, C.; Barrutia, H.; Bou-Ali, M. M.; Ecenarro, O.; Valencia, J. J. *Cr. Mecanique* **2011**, *339*, 292−296.
(28) Köhler, W.; Rossmanith, P. *J. Phys. Chem.* **1995**, *99*, 5838−5847.
(29) Wiegand, S.; Ning, H.; Kriegs, H. *J. Phys. Chem. B* **2007**, *111*, 14169−14174.
(30) Kolodner, P.; Williams, H.; Moe, C. *J. Chem. Phys.* **1988**, *88*, 6512−6524.